Analysis of Low-Frequency Phonons in Guanosine Dihydrate Based on Molecular Dynamics Simulations

Shigetaka Yoneda,*,† Yoko Sugawara,† and Hisako Urabe‡

School of Science, Kitasato University, Kitasato, Sagamihara, Kanagawa 228-8555, Japan, and Tokyo Kasei Gakuin University, Aihara, Machida, Tokyo 194-0292, Japan

Received: February 27, 2008; Revised Manuscript Received: May 19, 2008

Fourier analysis, using the atomic trajectory calculated by molecular dynamics simulation at 300 K, is applied to the study of low-frequency phonons of guanine dihydrate. The vibrational modes of guanine bases are analyzed, and the optically active modes associated with the guanine moieties are extracted. There are a few significant peaks in the low-frequency region. A possible assignment of the Raman active mode near 27 cm^{-1}, whose origin would be common to the S-mode of DNA double helices, is discussed.

Introduction

Hydration water dynamics are of interest in connection with their contribution to the functional structures of biomolecules.[1,2] In the cases of hydrates, phase transitions are often caused by changes in the crystal water amount.[3] We are able to obtain information how hydration water affects structures of molecules and molecular assemblies, if the details of the phase transitions become clear. The phenomena have also been studied for the practical purpose of controlling transformations during the manufacture or storage of pharmaceuticals.[4] Phase transitions are investigated by spectroscopic measurements, thermal methods, and crystallographic analysis. Phonon analysis based on vibrational spectroscopy and the neutron inelastic scattering method is one of the most effective techniques.

The water content of nucleoside and nucleotide hydrates is known to be dependent on the relative humidity of the crystal environment.[5] On the other hand, the effects of water content on the structures of molecules and molecular assembly have remained somewhat unclear for a long while. Our group has been investigating the humidity-dependent phase transitions of nucleoside and nucleotide hydrates, such as disodium adenosine 5′-triphosphate (Na_2ATP),[6–8] guanosine,[7,9] and disodium cytidine 5′-monophosphate (Na_2CMP),[10] through crystallographic and thermodynamic analyses, nuclear magnetic resonance, and vibrational spectroscopy. These phase transitions were found to be accompanied by characteristic changes in the low-frequency Raman spectra.[7] The Raman spectra of the phonon region observed at the phase transition of guanosine are shown in Figure 1. A characteristic peak, several times stronger than any of the other peaks, is present at 27 cm^{-1} for the dihydrate. Upon transition to the anhydrous form, the lowest peak shifts to 21 cm^{-1}. It is at 32 cm^{-1} in the intermediate state M. There exists a similar mode in the low-frequency Raman spectra of the self-aggregate of guanosine, where planar tetramers of guanine bases stack in head-to-tail arrangement, and of the self-aggregates and crystals of nucleotides in which the base moieties are stacked uniformly in a long-range pattern.[11,12] It was therefore proposed that the modes may originate from the motion of bases stacked in a column and that shifts of this mode reflect the change of intercolumn interaction accompanying the phase transition. The origin of this peak is considered to be common with that of the "S-mode" vibrational peak observed at ca. 20 cm^{-1} in the Raman spectra of DNA.[12] The frequency of the S-mode shifts in the A−B transition of DNA.[13,14] Although it has been shown that the S-mode is not the rigorous "soft mode"[14] that corresponds to the main pathway of the A−B transition, the S-mode remains closely related to the A−B transition.

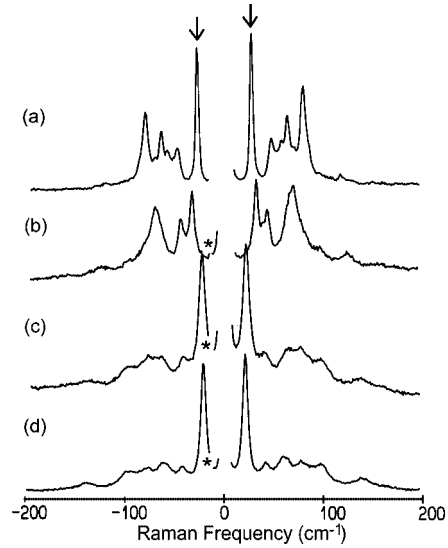

Figure 1. Low-frequency Raman spectra of guanosine: (a) dihydrate, (b) intermediate state M (ca. $1.2H_2O$), (c) intermediate state A′ (ca. $0.3H_2O$), and (d) anhydrate. S-mode-like phonons are indicated by arrows. The regions indicated by asterisks are omitted because spontaneous emissions were overlapped.

In a preceding study,[15] molecular dynamics (MD) simulations of guanosine dihydrate were performed in order to gain further understanding of the crystal dynamics and phase transitions of crystalline nucleosides. The structure and dynamics of the simulations are considerably accurate, as indicated by the good correspondence between the simulated and experimental structure and Debye−Waller temperature factors (*B*-factors).[16] In the present study, Fourier analysis of atomic trajectories calculated by MD simulations is conducted as a means of visualizing molecular vibrations. The characteristic Raman mode in the

* Corresponding author: Tel +81 42 778 9404; fax +81 42 778 9538; e-mail: syoneda@kitasato-u.ac.jp.
† Kitasato University.
‡ Tokyo Kasei Gakuin University.

10.1021/jp8017277 CCC: $40.75
Published on Web 07/09/2008

20−30 cm^{-1} region is then examined in detail in an attempt to assign the S-mode-like vibration.

The power spectrum of Raman scattering is equivalent to the Fourier transform of the time correlation function of molecular polarizability.[17] By the Wiener−Khinchin theorem, the Fourier transform of the time correlation function is identical to the squares of the absolute values of Fourier coefficients. The Raman spectrum can thus be calculated either by Fourier transformation of the time correlation function of polarizability or by direct Fourier transformation. However, a major obstacle in the calculation of the Raman spectrum is the difficulty in calculating polarizability, particularly in the case of phonon modes. Prediction of the infrared absorption spectrum, by contrast, is relatively straightforward, being calculable from the dipole moment, which can be readily determined by quantum chemistry.[18] With the conventional assumption that the polarizability is a constant specific to the rigid molecular structure, the change in polarizability should be proportional to the translational and rotational motion of the molecule. The power spectrum of Raman scattering is thus qualitatively predictable by Fourier transformation of the time correlation function of the motion of molecules and also by direct Fourier transformation or normal-mode analysis. However, normal-mode analysis of low-frequency modes is no easy matter because of a large anharmonicity effect. Fourier transformation of the time correlation function is beyond the scope of the present study, although such a refined analysis would provide a more quantitative estimation of numerical error and line shape than direct Fourier transformation.[19] Direct Fourier analysis is therefore employed here, focusing on the translation and rotational movements of bases to which the S-mode is expected to be related.

Theoretical Calculations

As the calculation conditions for the MD simulation have been reported in detail,[15] only the relevant conditions are briefly mentioned here. Simulations are performed by use of the AMBER 6 program[20] with AMBER ff99 energy parameters[21] and TIP3P water parameters.[22] As the total electrostatic charge of guanosine dihydrate is neutral, the particle-mesh Ewald method[23] is readily applicable to the calculation of electrostatic interactions.

The space group of guanosine dihydrate is $P2_1$, and the unit cell is composed of two asymmetric units, each of which contains two guanosine molecules (GA and GB) and four water molecules. The unit cell thus contains four guanosine molecules (GA1, GB1, GA2, and GB2) and eight water molecules. GA1 and GA2, and GB1 and GB2, are correlated by 2-fold screw axes. Figure 2 shows the four guanosine molecules in the unit cell. GA and GB are stacked in an alternating inverse manner to form columns along the *c* axis. Interbase hydrogen bonds are formed along the *b* axis between GA1 and GA2 and between GB1 and GB2.

The crystallographic unit cell in $P2_1$ symmetry with β angle of 98.17° is replicated four, five, and eight times in the *a*, *b*, and *c* directions, respectively, to form a parallelepiped with initial coordinates and side lengths of 70.072, 57.510, and 53.264 Å (Figure 3). The *X* and *Y* axes of Cartesian coordinates are oriented parallel to the crystallographic *a* and *b* axes, respectively, and the *Z* axis is declined with respect to the *c* axis by 8.17°. The periodic boundary box contains 160 unit cells and 320 asymmetric units, constituting 640 guanine bases. After energy minimization, the simulation is performed in time steps of 0.5 fs for 2 ns at 300 K with a relaxation time of 0.5 ps. The

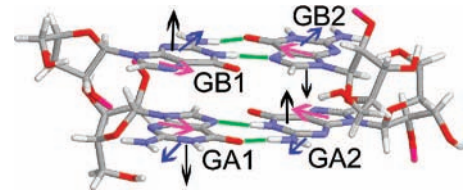

Figure 2. Four guanosine molecules (GA1, GB1, GA2, and GB2) in the unit cell with the definition of orientation vectors. Green lines denote hydrogen bonds between bases, and crystal water molecules are not shown. Pink arrows denote unit vector **V**1 from center of N9, C8, N3, and C4 to the center of N1, C5, and N7. Blue arrows denote unit vector **V**2 from the center of N9, C8, N7, and C5 to the center of C2, N2, C3, and C4. Black arrows denote vector **V**3, defined as **V**1 × **V**2. The directions of **V**2 and **V**3 for GB are the inverse of those for GA in Cartesian space, and the direction of **V**1 for GA1 and GB1 is the inverse of that for GA2 and GB2.

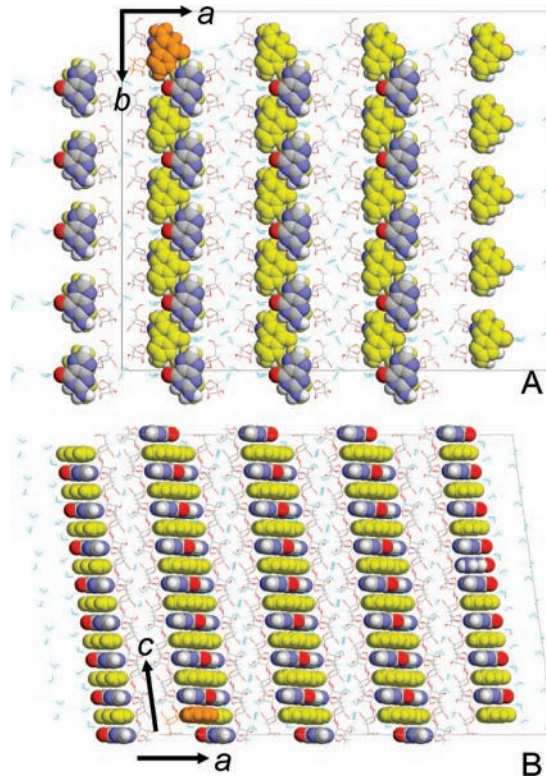

Figure 3. Initial structure for MD simulation of guanosine dihydrate: (A) viewed along the *c* axis and (B) viewed along the *b* axis. Periodic boundary box indicated by the parallelogram is made of four, five, and eight unit cells in the *a*, *b*, and *c* directions, respectively. Guanine bases are shown as space-filling models (yellow, GA; orange, GA1 in the first unit cell; CPK colors, GB), and other parts, including water molecules (cyan), are shown as wire-frame models.

atomic trajectory is stored as a binary file and processed by Fourier transformation at sampling intervals (Δt) of 5 fs. Translocations of crystal water occurred at 700 ps in the MD simulations.[15] The trajectory between 450 and 650 ps (the sampling period *T* of 200 ps) was therefore analyzed to avoid the influence of translocation on the Fourier transformation, and a total of 40 000 snapshots were taken.

The center of a base was defined as the simple average of the atomic coordinates of all atoms of the base except hydrogen. The orientation vectors **V**1, **V**2, and **V**3 are defined as shown in Figure 2. Within error of 10°, **V**1 is parallel to the glycosidic bond, and **V**2 is in the guanine base plane orthogonal to **V**1. **V**1, **V**2, and **V**3 are approximately oriented in the *X*, *Y*, and *Z* directions, respectively.

A simple discrete Fourier transformation with respect to time is then performed to give the Fourier coefficients $a_k(m)$ and $b_k(m)$:

$$a_k(m) = \frac{2}{N}\sum_{j=0}^{N-1} Q(j\Delta t, m) \cos\left(\frac{2\pi kj}{N}\right) \quad (1)$$

$$b_k(m) = \frac{2}{N}\sum_{j=0}^{N-1} Q(j\Delta t, m) \sin\left(\frac{2\pi kj}{N}\right) \quad (2)$$

Here $Q(j\Delta t,m)$ is the center or orientation vector of the base numbered m at time $t = j\Delta t$. The base number m is counted in a repeat of sequence of GA1, GB1, GA2, and GB2. N is the number of snapshots (40 000), and k is defined as an integer denoting the frequency f ($f = k/T$). The values of $a_0(m)$ and $b_0(m)$ are zero since $Q(j\Delta t,m)$ is defined as the deviation from the time average. The power spectral density (PSD), $I_k(m)$, is defined as

$$I_k(m) = [a_k(m)^2 + b_k(m)^2]/2 \qquad \text{for } k \neq 0 \quad (3)$$

and the sum of $I_k(m)$ is equal to the average of the square of $Q(j\Delta t,m)$ from Parseval's theorem, which states that the power computed in the domain of Fourier coefficients equals to the power of the function before Fourier transformation:

$$\frac{1}{N}\sum_{j=0}^{N-1} Q(j\Delta t, m)^2 = \sum_{k=1}^{N/2} I_k(m) \quad (4)$$

Because the sampling period T ($T = N\Delta t$) is 200 ps, the low-frequency limit of the Fourier transformation is 1/200 ps^{-1} = 0.17 cm^{-1}. Therefore, Fourier coefficients were calculated for 1/0.17 = 6.0 points in the range of 1.0 cm^{-1} so that the calculated PSD values were multiplied by 6.0 to express the density of power in the range of 1.0 cm^{-1} correctly. PSD is related to the more intuitive quantity of amplitude: half the square of amplitude is equal to the power. For example, when a vibrational amplitude of a center of base is 0.057 Å, the power is $0.057^2/2 = 1.6 \times 10^{-3}$ Å^2. When a rotational amplitude of a unit vector is 0.01 rad (0.57°), the terminal of the vector moves with amplitude of 0.01 Å so that the power of the vibration of the terminal is $0.01^2/2 = 5 \times 10^{-5}$ Å^2.

The coefficients of $a_k(m)$ and $b_k(m)$ are processed further by discrete Fourier transformation with respect to m to give the Fourier coefficients aa_{k,k_m}, ab_{k,k_m}, ba_{k,k_m}, and bb_{k,k_m}, which for $k_m \neq 0$ are as follows:

$$aa_{k,k_m} = \frac{2}{M}\sum_{m=0}^{M-1} a_k(m) \cos\left(\frac{2\pi k_m m}{M}\right) \quad (5)$$

$$ab_{k,k_m} = \frac{2}{M}\sum_{m=0}^{M-1} a_k(m) \sin\left(\frac{2\pi k_m m}{M}\right) \quad (6)$$

$$ba_{k,k_m} = \frac{2}{M}\sum_{m=0}^{M-1} b_k(m) \cos\left(\frac{2\pi k_m m}{M}\right) \quad (7)$$

and

$$bb_{k,k_m} = \frac{2}{M}\sum_{m=0}^{M-1} b_k(m) \sin\left(\frac{2\pi k_m m}{M}\right) \quad (8)$$

For $k_m = 0$, $aa_{k,0} = (1/M)\sum_{m=0}^{M-1} a_k(m)$, $ab_{k,0} = 0$, $ba_{k,0} = (1/M)\sum_{m=0}^{M-1} b_k(m)$, and $bb_{k,0} = 0$. Here k_m denotes the wavenumber and $1/\lambda = k_m/M$ ($M = 640$), where λ is the wavelength in units of sequential numbers of bases in the boundary box. The PSD, I_{k,k_m}, for vibration with k and k_m is calculated as follows:

$$I_{k,k_m} = (aa_{k,k_m}{}^2 + ab_{k,k_m}{}^2 + ba_{k,k_m}{}^2 + bb_{k,k_m}{}^2)/4 \qquad \text{for } k_m \neq 0 \quad (9)$$

$$I_{k,k_m} = (aa_{k,k_m}{}^2 + ba_{k,k_m}{}^2)/2 \qquad \text{for } k_m = 0 \quad (10)$$

Fourier analysis was performed with the simulated trajectory of atomic coordinates. Similar analyses can be performed with the atomic velocity, which is a time derivative of coordinates, such that the Fourier transformation of velocity should give similar results with larger PSD at higher frequencies. Preliminary calculations indicated that the Fourier transform of velocity is much noisier for the low-frequency vibrations considered in this paper, and thus the trajectory of atomic coordinates was used throughout the present investigation.

Results

Average Power Spectrum Density of Translational and Rotational Movements of Base Moieties. Figure 4 shows the average PSDs, $\sum_{m=0}^{M-1} I_k(m)/M$, for vibration of the center of nine

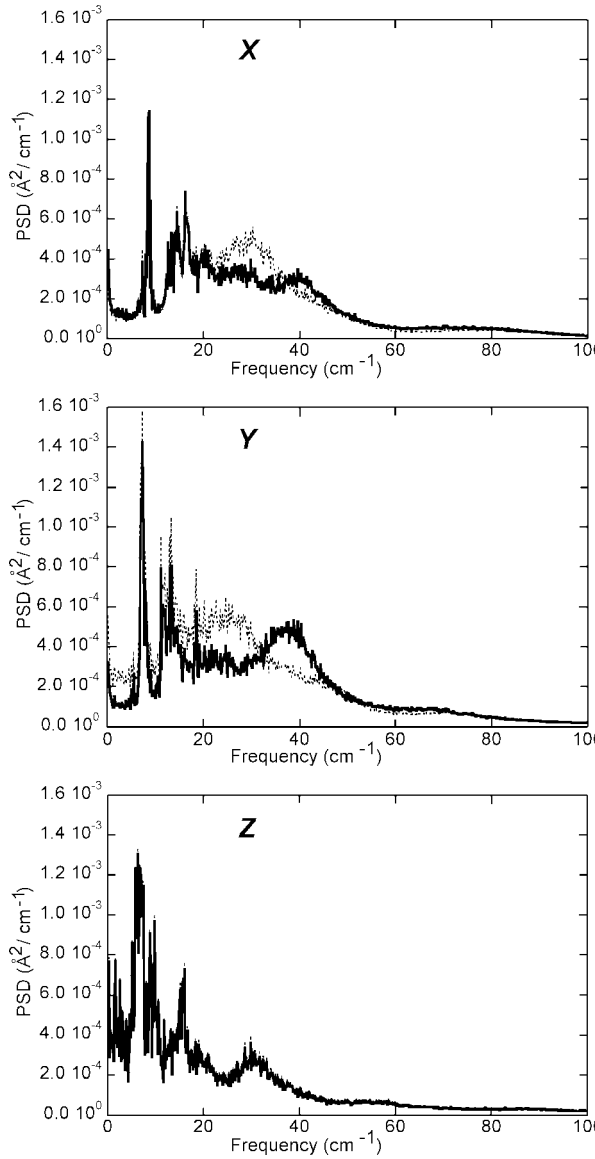

Figure 4. Average PSD spectra of translational vibrations of the base center of GA (solid lines) and GB (dotted lines) along the *X*, *Y*, and *Z* directions. PSDs decrease monotonically with increasing frequency beyond 100 cm^{-1} with some numerical noise.

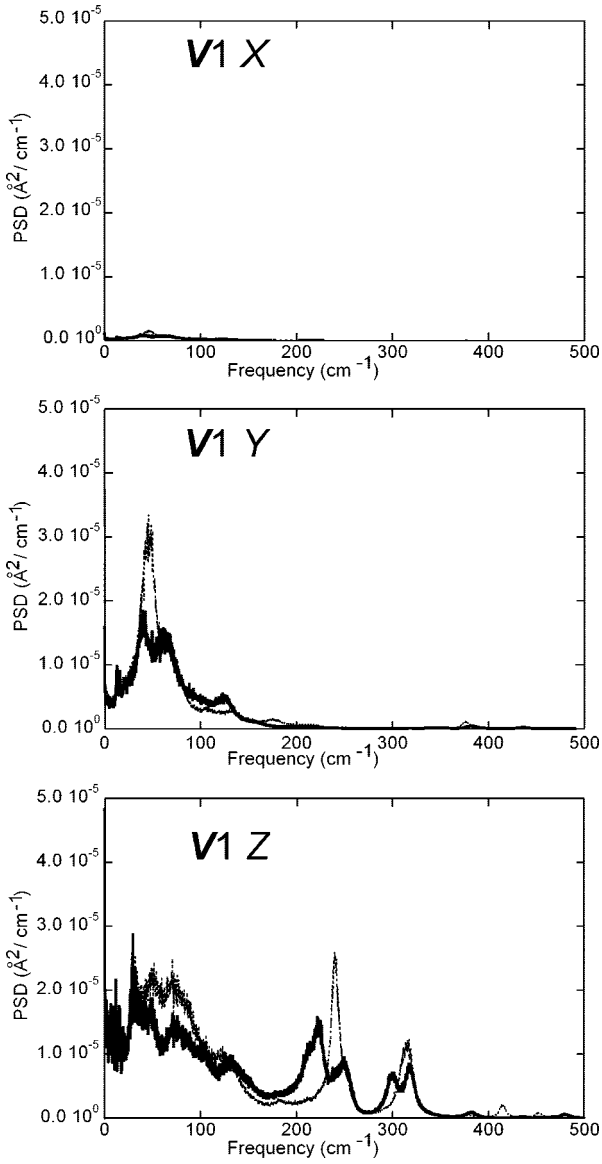

Figure 5. Average PSD spectra for the rotational vibrations of bases, **V**1 *X*, **V**1 *Y*, and **V**1 *Z*. The spectra of GA and GB are shown as solid and dotted lines, respectively. The PSD of **V**1 *X* is very small because vibration of the unit vector cannot occur parallel to the direction of the vector itself.

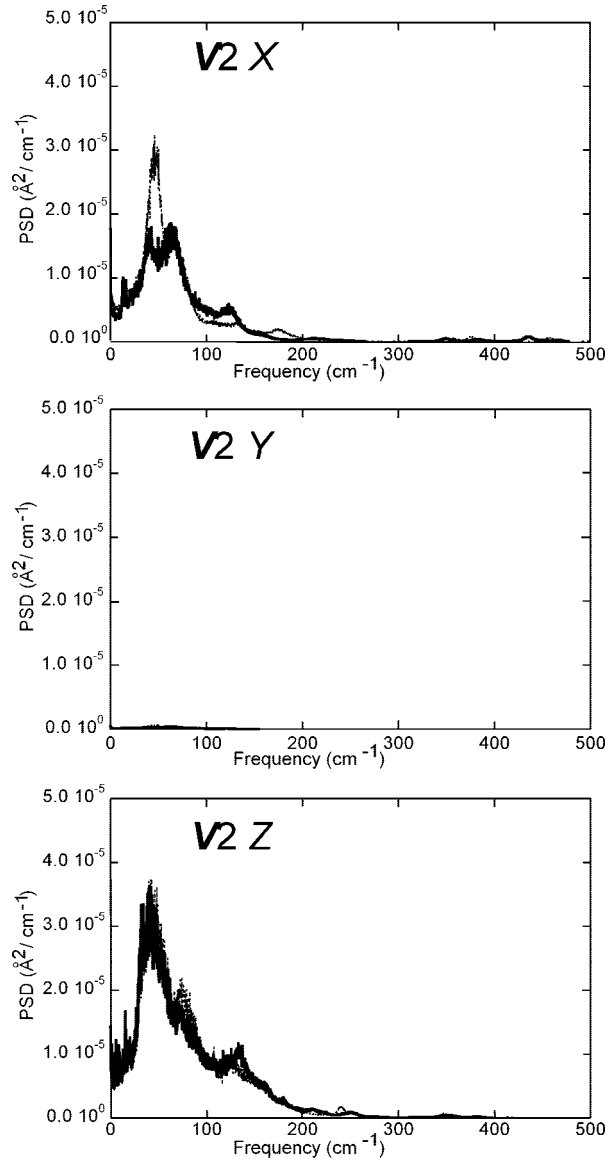

Figure 6. Average PSD spectra for the rotational vibrations of bases, **V**2 *X*, **V**2 *Y*, and **V**2 *Z*. The spectra of GA and GB are shown as solid and dotted lines, respectively. The PSD of **V**2 *Y* is very small because vibration of the unit vector cannot occur parallel to the direction of the vector itself.

atoms (N1, C2, N3, C4, C5, C6, N7, C8, and N9) of bases GA and GB. The PSDs of the *X* and *Y* vibrations of GA and GB are somewhat different, whereas the Z vibrations of GA and GB are almost identical.

Figures 5–7 show the average PSDs for the rotational vibration of the orientation vectors. The PSDs decrease monotonically at frequencies greater than 500 cm^{-1} with some numerical noise. PSDs for the **V**1 *Y* and **V**2 *X* components are almost identical, representing the same in-plane twist of guanine bases. There is a similar identity between **V**2 *Z* and **V**3 *Y* and between **V**1 *Z* and **V**3 *X*. Therefore, the analysis of rotational vibration can be restricted to the in-plane twist of bases (**V**1 *Y*), the hinge motion of the vector of the glycosidic bond in the *Z* direction (**V**1 *Z*), and the screw rotation around the glycosidic bond (**V**2 *Z*).

The spatial distribution of vibration phases can be depicted by extracting phases from the Fourier coefficients $a_k(m)$ and $b_k(m)$. Figure 8 shows the phase distributions for the translational vibrations of the center at 30 cm^{-1} and for rotational vibrations of the orientation vectors at 40 cm^{-1} within the periodic boundary box. Figure 8 (*Z*) demonstrates that there is a longitudinal wave whose wavelength is approximately 16 bases along the column direction (eight unit cells along the *c* axis). The vibration of **V**2 *Z* has a wavelength of approximately two bases. The bases of GA and GB stack alternatively along the *Z* direction; therefore the phase difference between GA and GB is 180°. Because the direction of **V**2 for GB is the reverse of that for GA (Figure 2), the phase difference of 180° for **V**2 *Z* indicates that the rotational directions of GA and GB around the glycosidic bonds are the same.

The phase distribution along the column direction is analyzed by use of an integer *s* denoting the sequential base number in a column. Figure 9 shows the wavenumber−frequency plots, which would correspond to the neutron inelastic observations for the directions of *c**. Figure 9 (*X*) and (*Y*) correspond to the transverse waves, whose vibrational directions are along the *a* and *b* axes, respectively, and the propagative direction is along the *c** axis. Figure 9 (*Z*) is the longitudinal wave along the *c**

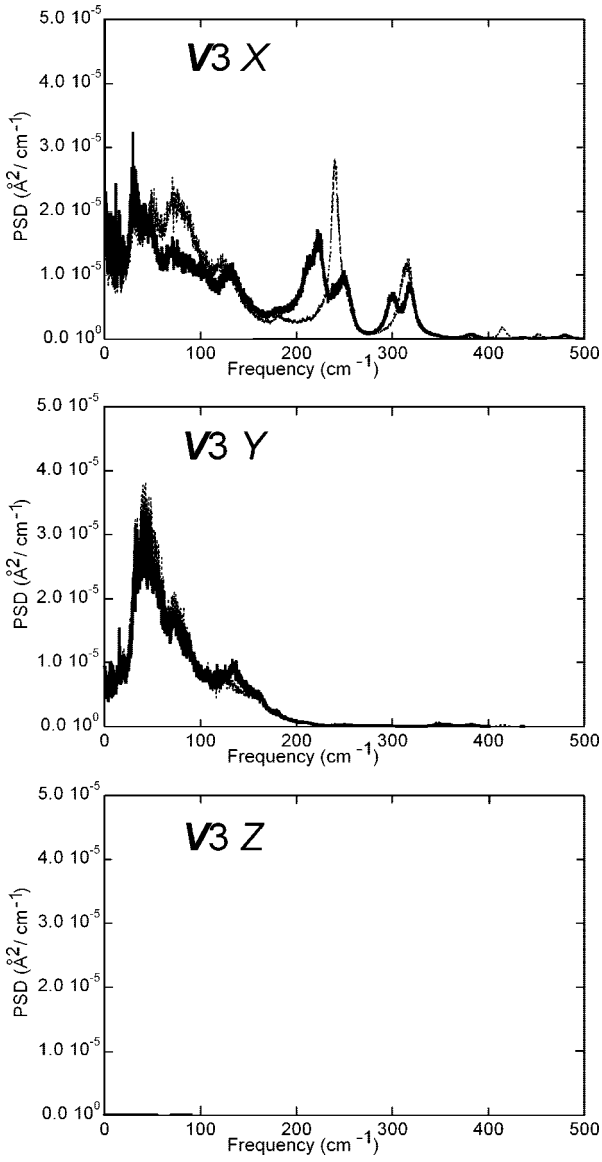

Figure 7. Average PSD spectra for the rotational vibrations of bases, **V**3 *X*, **V**3 *Y*, and **V**3 *Z*. The spectra of GA and GB are shown as solid and dotted lines, respectively. The PSD of **V**3 *Z* is very small because vibration of the unit vector cannot occur parallel to the direction of the vector itself.

axis. The slope of the curve of frequency versus k_s in *Z* is steeper than those in *X* and *Y*. A peak appears near 30 cm^{-1} in Figure 9 (*Z*), with k_s of 1 ($\lambda_s = 16$, $k = c^*/8$), where k_s and λ_s denote the wavenumber and wavelength in the column direction, respectively. This peak corresponds to the wave demonstrated in Figure 8 (*Z*).

The collective motions of atoms, vibrational waves, and the phonon dispersion along the c^* axis are shown in Figures 4–9. The information pertains to the motion of atomic nuclei and thus contributes to a more comprehensive understanding of phonons observed by neutron inelastic scattering.

The *X*, *Y*, *Z* vibrations of centers in guanosine molecules and ribose moieties were also investigated in the same manner (data not shown). The spectra for guanosine are very similar to those for the guanine moieties. Similar Fourier analysis of water molecules produced no clear spectrum for water vibration, indicating that the water motion is too large to be expressed as a harmonic vibration around the average positions.

Optically Active Phonon Modes. The vibrational modes shown in Figure 9 are the averages among the columns and

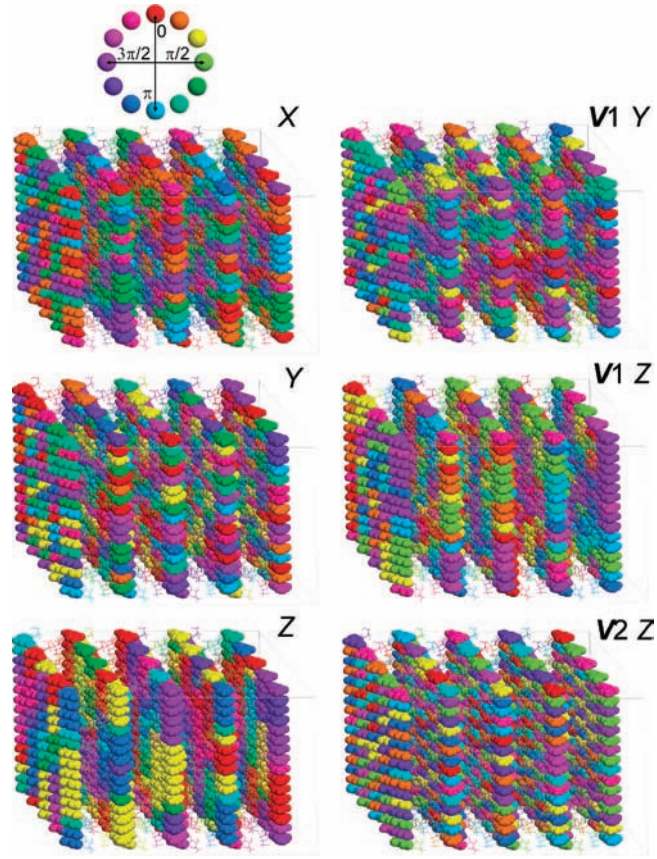

Figure 8. Phase distribution of the vibrations within the periodic boundary box. The vibrations of *X*, *Y*, and *Z* coordinates at 30 cm^{-1} (left) and **V**1 *Y*, **V**1 *Z*, and **V**2 *Z* components at 40 cm^{-1} (right) are shown. Base moieties are drawn as space-filling models, and other parts including water molecules are drawn as wire-frame models. The phase angles are indicated by hues of bases. The index between phase angles and colors is shown at the top.

thus represent mixtures of phonon modes. As the wavelength of light is much longer than the lattice size, the optically active modes that can interact with light are expected to be related to the vibration waves in that the optically equivalent molecules have identical phases in all the unit cells.[24,25] Therefore only the vibrations with $k_m = 0$, $M/2$ (i.e., 320), or $M/4$ (i.e., 160) are optically active, considering that four bases (GA1, GB1, GA2, and GB2) form the unit cell. When k_m is zero, λ is infinite and all bases have the same phase of vibration. When k_m is 320, the wavelength spans two guanine bases ($\lambda = 2$) such that the phases of all GA bases should be the same and those of all GB bases should be the same, as shown in Figure 10. When k_m is 160, the wavelength spans four guanine bases ($\lambda = 4$) and the respective phases of all bases (GA1, GB1, GA2, and GB2) are the same in each group of bases. GA1 and GA2 move in a reciprocal manner, as do GB1 and GB2. However, GA1 and GB1 can move either in phase or in the opposite manner, and thus the mode with k_m of 160 is divided into 160A (GA1 and GB1 move reciprocally) and 160B (GA1 and GB1 move in phase). From the Fourier transform of eqs 5–8, the vibrations with k_m of 0, 160, and 320 are presented with a constant, cos (2π 160*m*/640) and sin (2π 160*m*/640) and cos (2π 320*m*/640) and sin (2π 320*m*/640), respectively. The mode with $k_m = 320$ has only a single degree of freedom, cos (2π 320*m*/640), because sin (2π 320*m*/640) should be zero for any *m*. In contrast, the mode with $k_m = 160$ has two degrees of freedom (A and B)

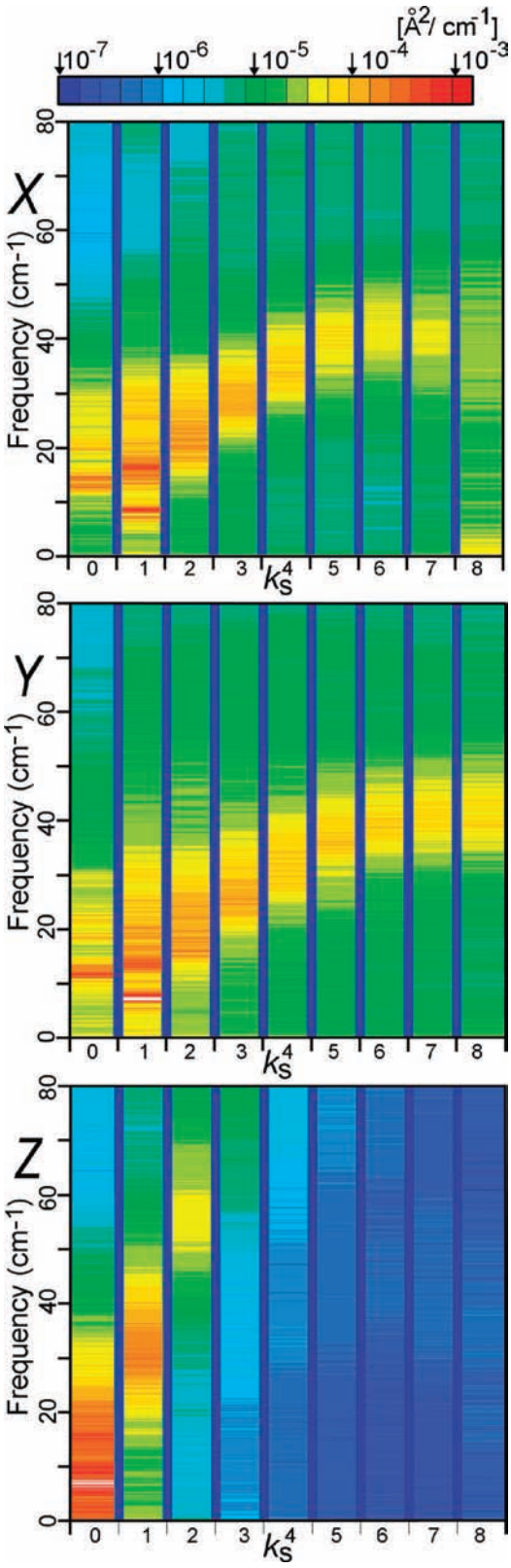

Figure 9. Wavenumber−frequency plots of vibrational waves *X*, *Y*, and *Z* along the *c** direction. The k_s value corresponds to the wavenumber that exists in the boundary box. The PSD values are represented by colors in a logarithmic scale shown on the top bar.

described by two independent functions, cos (2π 160*m*/640) + sin (2π 160*m*/640) and cos (2π 160*m*/640) − sin (2π 160*m*/640).

Figure 11 shows a schematic of the motion in the optically active *Z* vibration mode. The motion in the optically active *X* and *Y* vibration modes can be drawn similarly. Figures 12–14 show the motion in the optically active rotational modes, which are more complicated than the mode in Figure 11.

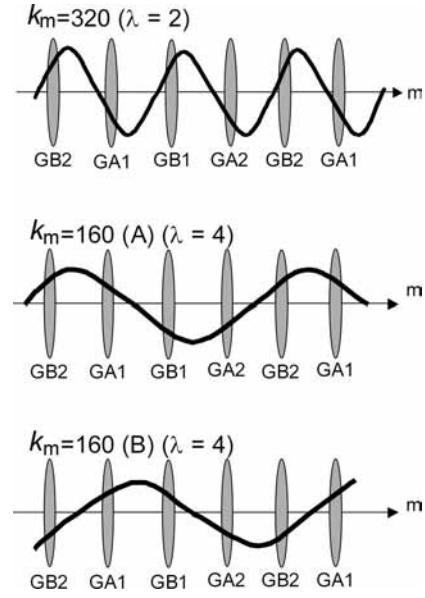

Figure 10. Phase of motion in waves with k_m of 320 and 160A,B. Ovals indicate the recurrence of bases, and displacements along the vibrational coordinates in the three modes are shown schematically as transverses.

The calculated PSDs of these modes are shown in Figures 15 and 16. The *X* and *Y* translational modes with $k_m = 320$, which maintain the relative position of the hydrogen-bonded bases, can be identified in the spectrum. The absence of a PSD peak in the frequency region corresponding to **V**1 *Y* in Figure 16 indicates that *X* and *Y* vibrations with $k_m = 320$ represent pure translations of the rigid body of the hydrogen-bonded bases with no rotation. The hydrogen-bonded GA1 and GA2 bases move in the inverse direction to GB1 and GB2 in the *X* and *Y* vibrations with $k_m = 320$. The PSD spectra are broad because the potential surface is shallow and wide for large rigid bodies. *Z* vibration with $k_m = 160$B produces a large PSD peak representing translation of the stacked bases in a direction orthogonal to the base plane. The movement of a column of GA1 and GB1 occurs in the reverse direction to that of a column of GA2 and GB2 in this mode, representing out-of-plane bending of the interbase hydrogen bonds.

The rotational vibration of **V**1 *Z* with $k_m = 0$ occurs such that the stacked bases remain parallel and the stacking distance remains constant, producing a PSD peak in Figure 16. The corresponding change of the *Z* translations with $k_m = 0$ is seen in Figure 15. **V**2 *Z* vibration with $k_m = 160$A is the other rotational vibration that maintains the parallelism of stacked bases to produce a PSD peak. This mode accompanies out-of-plane bending of the hydrogen bonds. The second mode of the **V**2 *Z* vibration with $k_m = 160$B corresponds to rotational vibration in which the stacking distance changes, resulting in a negligible PSD response in the frequency region shown in Figure 16.

Excepting the *X*, *Y*, and *Z* translations with k_m of 0, the frequencies of which should be zero, 21 modes are expected. However, only three vibrations, *Y* with $k_m = 320$, *Z* with $k_m = 160$B, and **V**2 Z with $k_m = 160$A, are clear in the calculated PSD spectra. The *X* vibration with $k_m = 320$ and the **V**1 *Z* vibration with $k_m = 0$ are split into several modes. Some of the vibrations, such as *X* and *Y* translations with $k_m = 160$A/B and

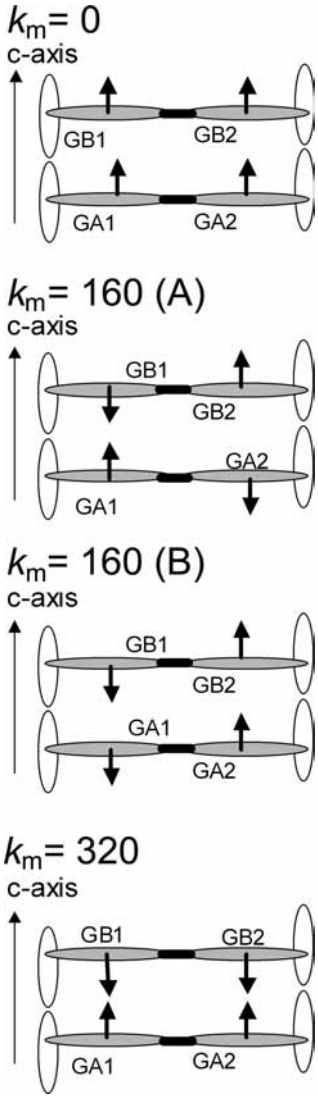

Figure 11. Schematic illustration of Z vibrations with $k_m = 0$, 160A, 160B, and 320. Molecular motion is depicted by arrows, and guanine bases and riboses are denoted by solid and open ovals, respectively. Hydrogen bonds between base pairs forming the base layer are denoted by thick solid black lines.

V1 Y rotation with any k_m value, accompany the stretching and/or in-plane bending modes of hydrogen bonds, and their frequencies would be much higher. The base and ribose moieties of stacked molecules are hydrogen-bonded, and the Z vibration with $k_m = 320$ accompanies the hydrogen-bond stretching.[16] The rotational vibrations involving changes in stacking distance would also appear at higher frequency in the PSD spectra. Other vibrations might be coupled with low-frequency intramolecular modes, such as torsional vibrations around the glycosidic bonds or the pseudorotational modes of ribose moieties. The base motions illustrated in Figures 13 and 14 may split into several modes.

Discussion

Although the humidity-dependent phase transitions of nucleoside and nucleotide crystals were identified through gravity measurements soon after discovery of the A−B transition of DNA,[5] the details of the transitions have yet to be clarified in detail. Our group has therefore investigated the phase transitions of nucleoside and nucleotide hydrates by crystallographic analysis and Raman spectroscopy.[6–10] It

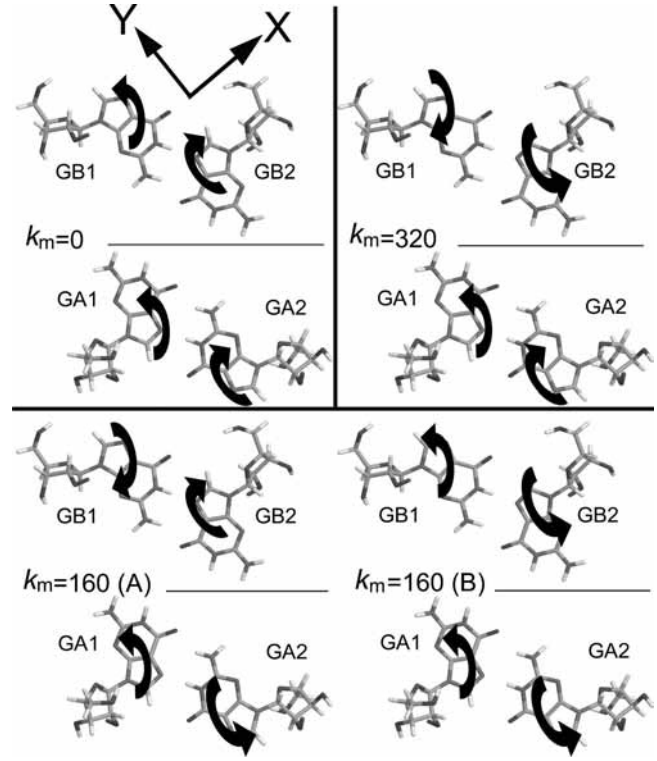

Figure 12. Phase of motion of optically active **V**1 Y vibration. The directions of the X and Y axes are depicted by arrows at the upper left corner. The motion of **V**1 vector, rotating to the Y direction, is depicted by an arrow. GA1 and GB1, and GA2 and GB2, are respectively stacked in three-dimensional space. The mode with $k_m = 160$ consists of two kinds of motion.

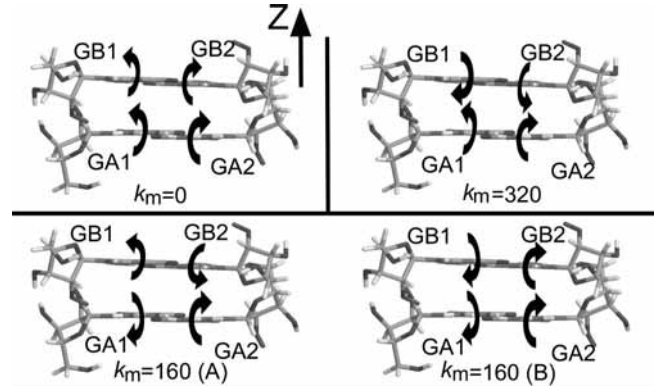

Figure 13. Phase of motion in optically active **V**1 Z vibration. Four molecules in a unit cell are viewed along the Y direction, and the motions in each mode are indicated by arrows.

was revealed that characteristic shifts of the low-frequency Raman modes occurred.

Clarification of the experimentally detected vibrations requires the assignments. However, in the study of crystalline organic molecules, the theoretical assignment of low-frequency spectra is relatively difficult except in cases of simple or rigid molecules. In all other cases, several intramolecular vibrations are typically present in the low-frequency region, and couplings between intermolecular and intramolecular vibrations need to be taken into account. Anharmonic effects can also complicate normal-mode analysis. The Fourier analysis of atomic trajectories calculated by MD calculations introduced in the present study allows these molecular vibrations to be visualized without the complications.

The results shown in Figures 4–9 clarify the collective motion of atoms, vibrational waves, and dispersion of phonons in the

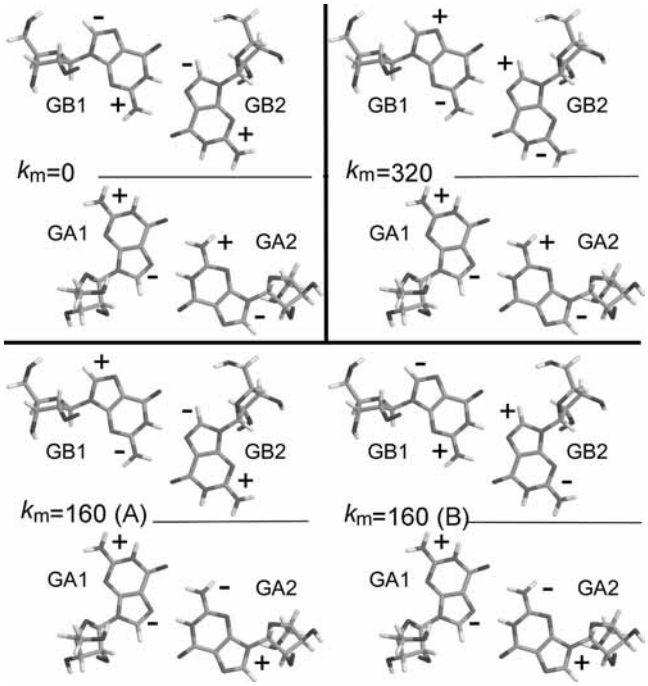

Figure 14. Phase of motion in optically active **V**2 *Z* vibration. Positive and negative signs denote the motions orthogonal to the page.

guanosine dihydrate crystal. This information is expected to contribute to a comprehensive understanding of phonons observable by neutron inelastic scattering.

The optically active modes assigned to the motions of bases were picked up by further discrete-Fourier transformation with respect to *m*. Three types of vibrations were identified: *Y* translation with $k_m = 320$ (35−45 cm^{-1}), *Z* translation with $k_m = 160$B (ca. 25 cm^{-1}), and **V**2 *Z* rotation with $k_m = 160$A (ca. 37 cm^{-1}). *X* translation with $k_m = 320$ and **V**1 *Z* rotation with $k_m = 0$ were split into several modes. Considering the good correspondence between the simulated and experimental temperature factors,[15] which is in close relation with phonons, the atomic trajectories determined through the simulations are expected to be reliable. The translational vibration of stacked bases in the direction orthogonal to the base plane (*Z* with k_m=160B), the translational vibrations where the stacked bases slide to the opposite sides along the short axes (*X* with $k_m = 320$), and the rotational vibration where the hydrogen-bonded bases rotate to the opposite sides (**V**1 *Z* with $k_m = 0$) are likely candidates for the characteristic Raman mode observed at 27 cm^{-1}. The space group of guanosine dihydrate is $P2_1$; then k_m of 0 and 320 belong to representation A and k_m of 160 belongs to representation B of the crystal point group of C_2. They would be distinguished in polarized infrared or Raman spectra, although observation of polarized spectra has not succeeded at present due to the small crystal size. The origin of the low-frequency modes of DNA has been discussed on the basis of both experimental[14,27–30] and theoretical studies.[31–34] However, a definitive model for the S-mode has yet to be established. A series of investigations of low-frequency Raman spectra of nucleoside and nucleotide hydrates and self-aggregates indicated that the origin of the characteristic Raman peak at 27 cm^{-1} of guanosine dihydrate is closely related to that of the S-mode of DNA.[12] Therefore, the present analysis suggests that the S-mode is attributable to one of the above-mentioned modes.

Although low-frequency vibrations provide valuable information on polymorphism and phase transitions, analysis

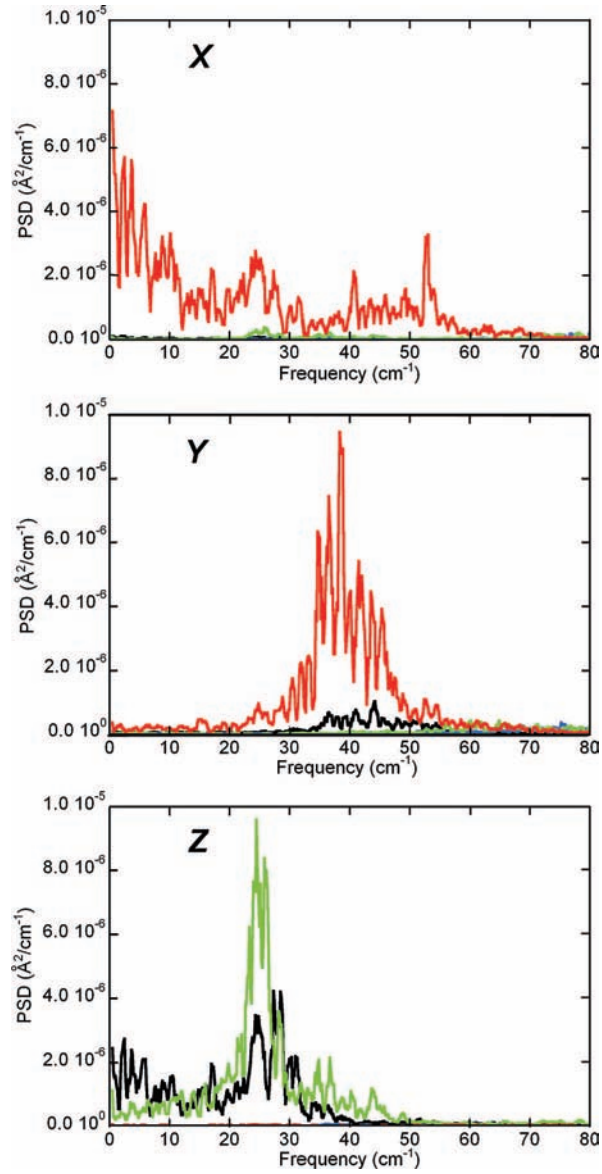

Figure 15. PSD spectra of translational vibrations of bases with k_m of 0 (black), 160A (blue), 160B (green), and 320 (red). Smoothing is applied over five contiguous points by use of the Stineman function.[26] The PSDs of the *X*, *Y*, and *Z* with $k_m = 160$A are very small compared to the other modes and are hardly seen in these figures.

of such vibrations is difficult in organic crystals. However, the present approach appears helpful for analysis of low-frequency Raman spectra, as demonstrated for the case of guanosine. It is suggested that only a few optically active modes are described as pure translational or rotational vibrations at 300 K.

Conclusion

The atomic motions of guanosine dihydrate were analyzed by Fourier transformation of the atomic trajectory calculated by MD simulations. The derived power spectrum is expected to assist in the interpretation of neutron inelastic scattering. With the analysis restricted to optically active modes, five modes are clearly apparent in the calculated PSD spectra. When the observed and calculated frequencies are considered, the three modes producing a PSD response are suggested to

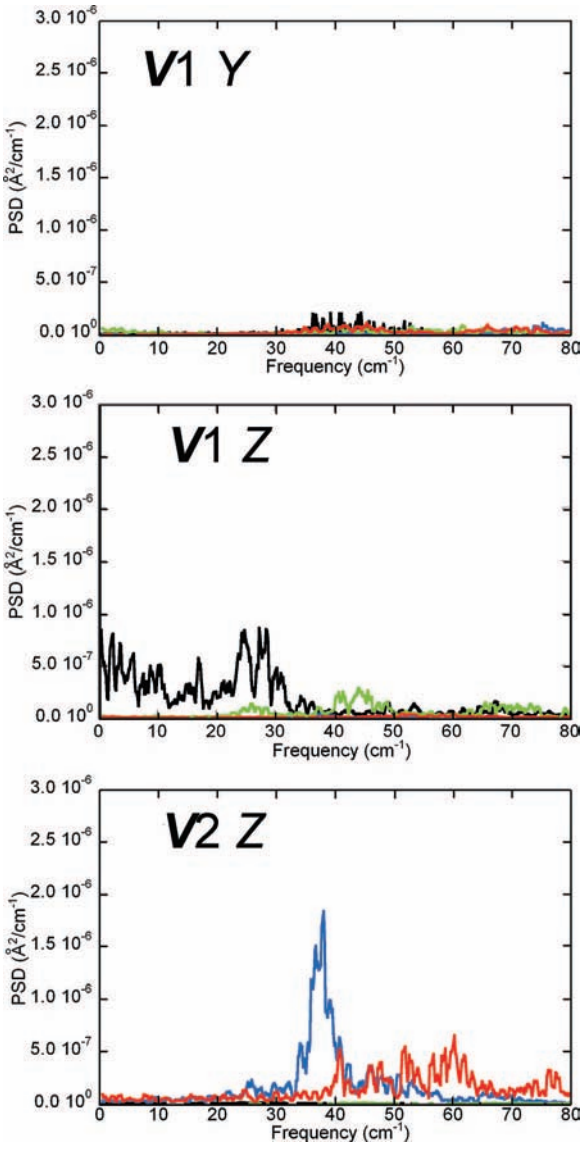

Figure 16. PSD spectra for orientation vectors of bases with k_m of 0 (black), 160A (blue), 160B (green), and 320 (red lines). Smoothing is applied over five contiguous points by use of the Stineman function.[26]

be candidates for the S-mode, which reflects the change in intermolecular interactions closely coupled with hydration.

Acknowledgment. This work was supported in part by Grants-in-Aid for Scientific Research (KAKENHI) from the Ministry of Education, Culture, Sports, Science and Technology of Japan.

References and Notes

(1) Rupley, J. A.; Careri, G. *Adv. Protein Chem.* **1991**, *41*, 37–172.
(2) Saenger,W. *Principles of Nucleic Acid Structure*; Springer-Verlag: New York,1983.
(3) Bernstein, J. *Polymorphism in Molecular Crystals*; Oxford University Press: New York, 2002.
(4) *Polymorphism in Pharmaceutical Solids*; Brittain, H. G., Ed.; Marcel Dekker: New York, 1999.
(5) Falk, M. *Can. J. Chem.* **1965**, *43*, 314–318.
(6) Sugawara, Y.; Kamiya, N.; Iwasaki, H.; Ito, T.; Satow, Y. *J. Am. Chem. Soc.* **1991**, *113*, 5440–5445.
(7) Urabe, H.; Sugawara, Y.; Kasuya, T. *Phys. Rev. B* **1995**, *51*, 5666–5672.
(8) Shindo, Y.; Naito, A.; Tuzi, S.; Sugawara, Y.; Urabe, H.; Saito, H. *J. Mol. Struct.* **2002**, *602*−*603*, 389–397.
(9) Sugawara, Y.; Iimura, Y.; Iwasaki, H.; Urabe, H.; Saito, H. *J. Biomol. Struct. Dyn.* **1994**, *11*, 721–729.
(10) Sugawara, Y.; Nakamura, A.; Iimura, Y.; Kobayashi, K.; Urabe, H. *J. Phys. Chem. B* **2002**, *106*, 10363–10368.
(11) Urabe, H.; Sugawara, Y.; Tsukakoshi, M.; Ikegami, A.; Iwasaki, H.; Kasuya, T. *Biopolymers* **1987**, *26*, 963–971.
(12) Urabe, H.; Sugawara, Y.; Tsukakoshi, M.; Kasuya, T. *J. Chem. Phys.* **1991**, *95*, 5519–5523.
(13) Urabe, H.; Sugawara, Y.; Ataka, M.; Rupprecht, A. *Biophys. J.* **1998**, *74*, 1533–1540.
(14) Lindsay, S. M.; Lee, S. A.; Powell, J. W.; Weidlich, T.; DeMarco, C.; Lewen, G. D.; Tao, N. J.; Rupprecht, A. *Biopolymers* **1988**, *27*, 1015–1043.
(15) Yoneda, S.; Sugawara, Y.; Urabe, H. *J. Phys. Chem. B.* **2005**, *109*, 1304–1312.
(16) Thewalt, U.; Bugg, C. E.; Marsh, R. E. *Acta Crystallogr.* **1970**, *B26*, 1089–1101.
(17) McQuarrie, D. A. *Statistical Mechanics*; Harper and Row: New York, 1973.
(18) Frankland, S. J. V.; Maroncelli, M. *J. Chem. Phys.* **1999**, *110*, 1687–1710.
(19) Kleinhesselink, D.; Wolfsberg, M. *Surf. Sci.* **1992**, *262*, 189–207.
(20) Case, D. A.; Pearlman, D. A.; Caldwell, J. W.; Cheatham, T. E., III; Ross, W. S.; Simmerling, C. L.; Darden, T. A.; Merz, K. M.; Stanton, R. V.; Cheng, A. L.; Vincent, J. J.; Crowley, M.; Tsui, V.; Radmer, R. J.; Duan, Y.; Pitera, J.; Massova, I.; Seibel, G. L.; Singh, U. C.; Weiner, P. K.; Kollman, P. A. *AMBER 6*; University of California, San Francisco, CA, 1999.
(21) Wang, J.; Cieplak, P.; Kollman, P. A. *J. Comput. Chem.* **2000**, *21*, 1049–1074.
(22) Jorgensen, W. L.; Chandrasekhar, J.; Madura, J. D.; Impey, R. W.; Klein, M. L. *J. Chem. Phys.* **1983**, *79*, 926–935.
(23) Essman, U.; Perera, L.; Berkowitz, M. L.; Darden, T.; Lee, H.; Pedersen, L. G. *J. Chem. Phys.* **1995**, *103*, 8577–8593.
(24) *Structure and Properties of Molecular Crystals*; Pierrot, M., Ed.; Elsevier: Amsterdam, 1990.
(25) Kittel,C. *Introduction to Solid State Physics*, 8th ed.; John Wiley and Sons: New York, 2005.
(26) Stineman, R. W. *Creative Computing* **1980**, *6* (7), 54–57.
(27) Weidlich, T.; Lindsay, S. M.; Rui, Q.; Rupprecht, A.; Peticolas, W. L.; Thomas, G. A. *J. Biomol. Struct. Dyn.* **1990**, *8*, 139–171.
(28) Wittlin, A.; Genzel, L.; Kremer, F.; Häseler, S.; Poglitsch, A. *Phys. Rev. A* **1986**, *34*, 493–500.
(29) Woods, K. N.; Lee, S. A.; Holman, H.-Y. N.; Wiedemann, H. *J. Chem. Phys.* **2006**, *124*, 224706.
(30) Grimm, H.; Rupprecht, A. *Physica B (Amsterdam, Neth.)* **1997**, *234*−*236*, 183–187.
(31) Saxena, V. K.; Van Zandt, L. L. *Phys. Rev. A* **1990**, *42*, 4993–4997.
(32) Chen, Y. Z.; Prohofsky, E. W. *Biopolymers* **1995**, *35*, 573–582.
(33) Lin, D.; Matsumoto, A.; Go, N. *J. Chem. Phys.* **1997**, *107*, 3684–3690.
(34) Cocco, S.; Monasson, R. *J. Chem. Phys.* **2000**, *112*, 10017–10033.

JP8017277